Supporting Information

Initiating highly efficient $(Bi,Ce)_2(O,S)_{3-x}$ oxysulfide catalyst with rich oxygen vacancies for hydrogen evolution via adjusting valence band configuration

Xiaoyun Chen[1,*], Qinhan Wu[1], Dong-Hau Kuo[2,*], Adugna Boke Abdeta[1], Hanya Zhang[1], Ping Li[1], Ting Huang[1], Osman Ahmed Zelekew[3], Jinguo Lin[1,*]

[1]College of Materials Engineering, Fujian Agriculture and Forestry University, Fuzhou 350002, China

[2]Department of Materials Science and Engineering, National Taiwan University of Science and Technology, Taipei 10607, Taiwan

[3]Department of Materials Science and Engineering, Adama Science and Technology University, Adama, Ethiopia

*Corresponding author

E-mail address: dhkuo@mail.ntust.edu.tw (D.-H. Kuo)

E-mail address: fjlinjg@126.com (J. G. Lin)

E-mail address: fjchenxy@126.com (X. Y. Chen)

Experimental Section

1. Apparent quantum efficiency computation

According to the literature reports [1, 2] for measuring the apparent quantum efficiency (AQE). In the experiment, the 420 nm (λ) monochromatic light, the 2.36 mW·cm^{-2} average intensity of irradiation (I), and the 32.15 cm^2 irradiation area (A) were used. The total H_2 evolution with 20 mg of BiCeOS catalyst was 473.75 μmol, which can be used to determine the number of reacted photons (N_{reac}). The number of photons (N_{in}) illuminated to reactor is computed according to the follow equations:

$$N_{in} = \frac{E \cdot \lambda}{h \cdot c} = \frac{(A) \cdot (I) \cdot (t) \cdot \lambda}{h \cdot c} = \frac{32.15 \times 2.36 \times 10^{-3} \times 3600 \times 5 \times 420 \times 10^{-9}}{6.626 \times 10^{-34} \times 3 \times 10^{8}} = 2.886 \times 10^{21}$$

$$AQE = \frac{N_{reac}}{N_{in}} \times 100\% = \frac{2 \times 6.02 \times 10^{23} \times 473.75 \times 10^{-6}}{2.886 \times 10^{21}} \times 100\% = 19.76\%$$

Where: *h*, *c*, and *t* are Planck constant, light speed under vacuum, and illumination time (s), respectively.

2. Density functional theory calculation

DFT computation was performed with the Vienna ab initio simulation package (VASP) by using the projector augmented wave (PAW) function method [3]. A plane-wave basis set was adopted to expand the smooth part of wave functions. The generalized gradient approximation (GGA) with Perdew–Burke-Ernzerhof (PBE) function was used for considering the electron exchange and correlation effect [4, 5]. A 2×2×2 supercell with 80 atoms was adopted for structures considered in this study. Dispersion correction (DFT-D3) proposed by Grimme was employed to accurately describe the Van-Der-Waals force. In the process of geometry optimization, atomic relaxation was

considered by referring to the Hellmann-Feynman force smaller than 0.02 eV/Å. The convergence criterion was set to have low energy of 1×10^{-5} eV during the electronic self-consistent loop. The Brillouin-zone integration used the gamma-centered (2×2×1) k-point grids for the geometry optimization [6].

3. Cycle voltammetry (CV) curve for calculation of conduction band (CB) and valence band (VB).

The CB and VB levels are calculated with the following Equations [7-9].

$$E_{CB} = -[4.8 + (E_{onset}^{ox} - E_{Ox})]\ eV \quad (1)$$

$$E_{VB} = -[4.8 + (E_{onset}^{red} - E_{Ox})]\ eV \quad (2)$$

where the E_{onset}^{ox}, E_{onset}^{red}, and E_{Ox} are the onset potentials for oxidation and reduction reaction of BiCeOS-3, and for the oxidation reaction of electrolyte, respectively.

Additional figures and tables

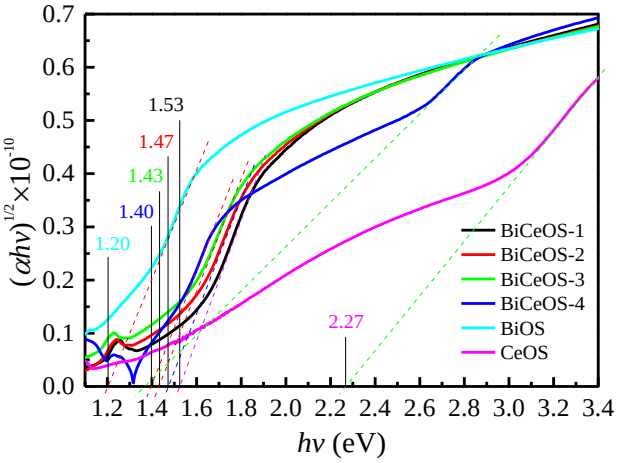

Fig. S1 the indirect bandgap $(\alpha h\nu)^{1/2}$ - $h\nu$ plot from the ultraviolet visible absorption spectra of CeOS, BiOS, and BiCeOS catalysts.

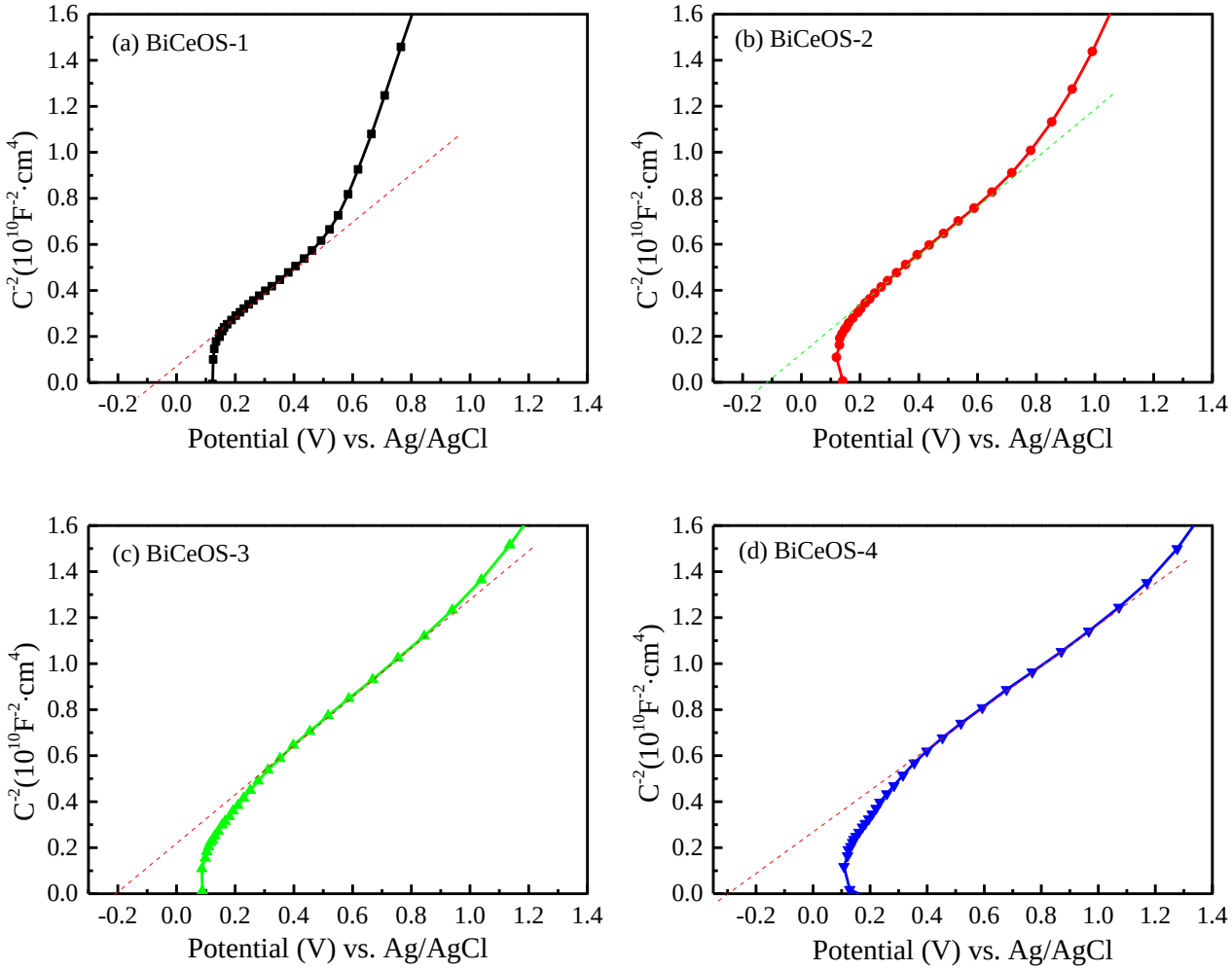

Fig. S2 Mott–Schottky curves of BiCeOS conducting at 1000 Hz.

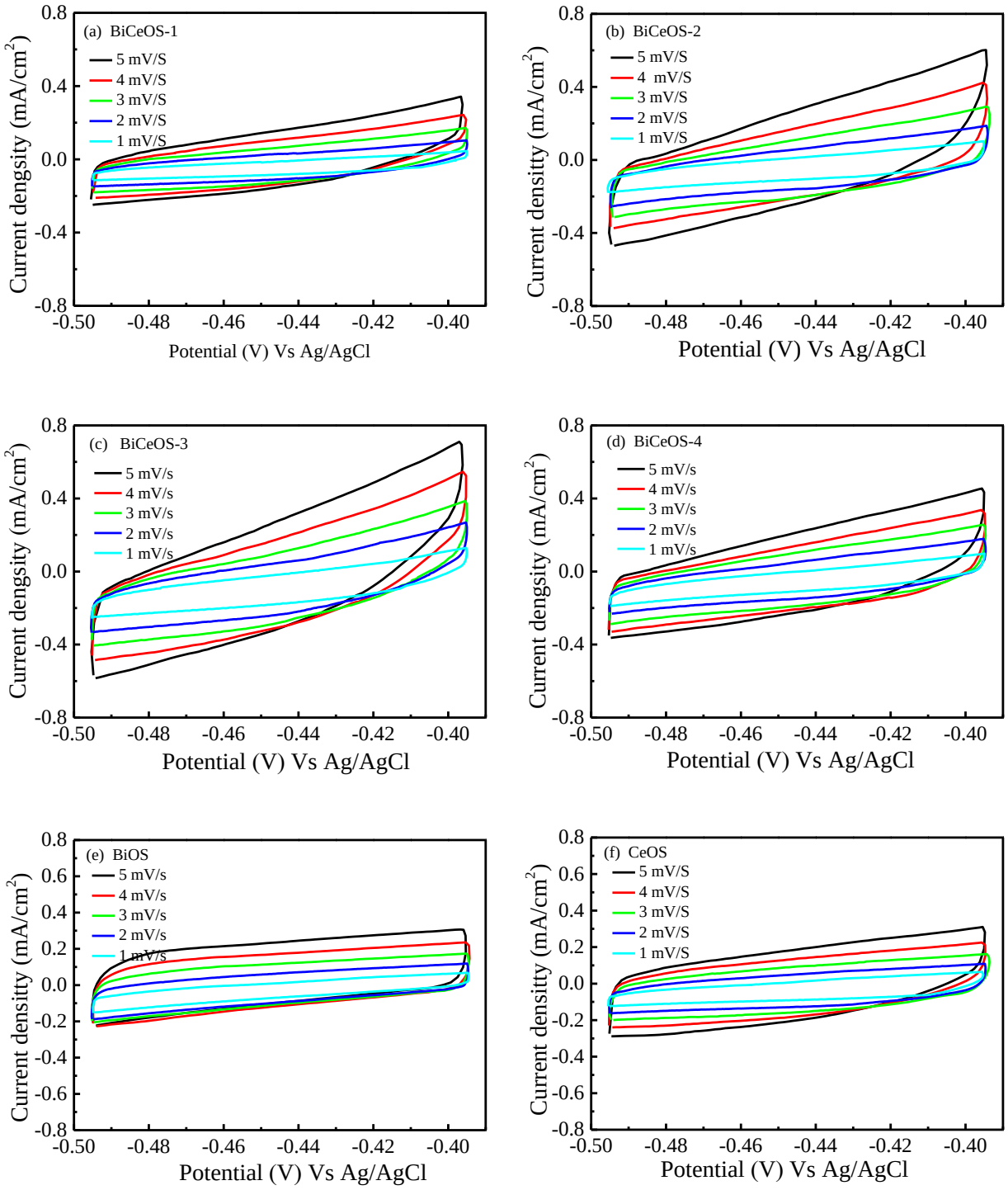

Fig. S3 Current density of BiCeOS, BiOS and CeOS under different scan rates.

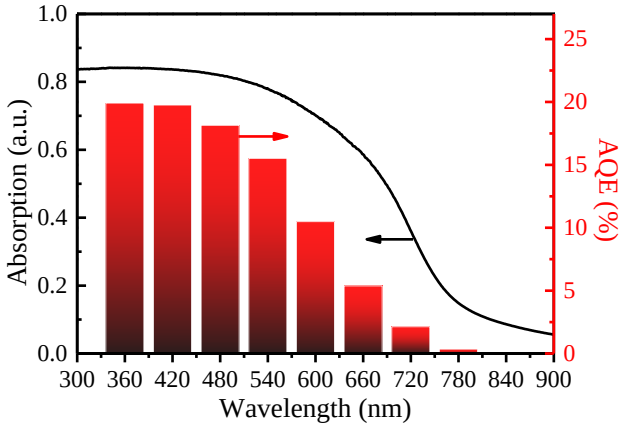

Fig. S4 The dependence of AQE as a function of irradiation wavelength and UV-Vis absorption spectrum of BiCeOS-3.

Table S1 XPS composition and physical characteristics of BiCeOS catalysts prepared with different N_2H_4 contents

Catalyst	Molar percentage/%				Ce molar percentage /%		Ce^{3+}/Ce^{4+} (%)	O molar percentage /%		$V_O/O_{Lattice}$ (%)	S_{BET} (m^2/g)	Crystal size/nm
	Bi	Ce	S	O	Ce^{3+}	Ce^{4+}		$O_{Lattice}$	V_O			
BiCeOS-1	37.28	6.07	41.28	15.37	3.12	96.88	3.22	97.39	2.61	2.68	31.2	10.7
BiCeOS-2	37.17	6.12	41.31	15.40	16.03	83.97	19.09	90.02	9.98	11.09	32.0	10.5
BiCeOS-3	37.25	6.09	41.17	15.49	39.52	60.48	65.34	84.52	15.48	18.32	30.5	11.0
BiCeOS-4	37.33	6.31	40.08	16.28	47.29	52.71	89.72	92.11	7.89	8.57	28.1	11.3
BiCeOS-3 after reaction	37.28	6.13	41.05	15.54	39.48	60.52	65.23	84.82	15.18	17.89	——	10.8

Table S2 Elements contents from SEM-EDS analysis for BiCeOS catalysts

Catalyst	Bi	Ce	S	O	Bi/Ce (%)
BiCeOS-1	36.18	5.67	40.26	17.89	15.67
BiCeOS-2	36.27	5.72	40.18	17.83	15.77
BiCeOS-3	36.00	5.63	40.32	18.05	15.64
BiCeOS-4	35.84	5.83	39.92	18.41	16.17

Table S3 The average charge carrier lifetime of BiCeOS catalysts

Catalysts	A_1	τ_1 (ns)	A_2	τ_2 (ns)	R^2	τ_{avg} (ns)
BiCeOS-1	51.961	1.946	1.406	5.172	0.991	2.162
BiCeOS-2	10.847	2.884	15.061	2.675	0.992	2.766
BiCeOS-3	9.712	3.097	12.528	3.956	0.996	3.632
BiCeOS-4	2.558	3.253	60.445	1.831	0.995	1.930
BiOS	2.181	5.636	587.359	0.928	0.992	1.032

Table S5 Reports on PHER performance over Bi-based and oxysulfide catalysts under visible light

Catalysts	**Sacrificial**	**Light source**	**AQE (%)**	**PHER rate (mmol/g·h)**	**Ref.**
Cr_2O_3/Rh/IrO_2@$Y_2Ti_2O_5S_2$	Na_2S/Na_2SO_3	300 W Xe lamp	5.3 (420 nm)	0.83	[10]
Pt/$La_5In_3S_9O_3$	Na_2S/Na_2SO_3	300 W Xe lamp	N/A (420 nm)	0.045	[11]
$ZnS_{1-x-0.5y}O_x(OH)_y$	Na_2S/Na_2SO_3	400 W halide lamp	3.0 (420 nm)	0.08	[12]
InOS	10 vol.% Ethanol	150 W Xe lamp	N/A	0.08	[13]
Ni-doped $Mo(S,O)_{3-x}$	10 vol.% Ethanol	250 W Xe lamp	29.2 (420 nm)	23.50	[14]
$(Ni,In)(S,O)_{2-x}$	10 vol.% Ethanol	250 W Xe lamp	26.3 (420 nm)	19.87	[15]
$Bi_5Ti_3CrO_{15}$	$NaSO_3$	300 W Xe lamp	3.6 (420 nm)	2.832	[16]
FeS_2/Bi_2S_3	Na_2S/Na_2SO_3	300 W Xe lamp	12.1 (420 nm)	16.8	[17]
$Cd_{0.5}Zn_{0.5}S$/Bi_2S_3	Na_2S/Na_2SO_3	300 W Xe lamp	19.6 (420 nm)	16.3	[18]
InBi-MOF	lactic acid	300 W Xe lamp	4.27 (420 nm)	3.6	[19]
Ru/$SrTiO_3$:Rh−(PRGO/$BiVO_4$)	MeOH	300 W Xe lamp	1.03 (420nm)	11.0	[20]
ZnO/Ag/Bi2S3	Na_2S/Na_2SO_3	250 W Hg lamp	1.1 (420nm)	0.218	[21]
Bi_2S_3/MoS_2/TiO_2	Na_2S/Na_2SO_3	250 W Xe lamp	N/A	2.23	[22]
Bi_2S_3/TiO_2	50 vol% methanol	300 W Xe lamp	N/A	2.46	[23]
MoS_2/P25/Bi_2S_3	10 vol% TEOA	350 W Xe lamp	N/A	2.33	[24]
BiOBr/Bi_2S_3	Na_2S/Na_2SO_3	300 W Xe lamp	N/A	0.445	[25]
BiCeOS	Na_2S/Na_2SO_3	250 W Xe lamp	19.8 (420 nm)	26.33	This work

References:

[1] Q. Huang, Y. Xiong, Q. Zhang, H. Yao, Z. Li, Noble metal-free MoS_2 modified $Mn_{0.25}Cd_{0.75}S$ for highly efficient visible-light driven photocatalytic H_2 evolution, *Appl. Catal. B-Environ.*, 209 (2017) 514-522.

[2] M.S. Nasir, G. Yang, I. Ayub, S. Wang, W. Yan, Tin diselinide a stable co-catalyst coupled with branched TiO_2 fiber and g-C_3N_4 quantum dots for photocatalytic hydrogen evolution, *Appl. Catal. B-Environ.*, 270 (2020) 118900.

[3] J.F. G. Kressea, Efficiency of ab-initio total energy calculations for metals and semiconductors using a plane-wave basis set, *Comp. Mater. Sci.*, 6 (1996) 15-50.

[4] K.B. J.P. Perdew, M. Ernzerhof, Generalized gradient approximation made simple, *Phys. Rev. Lett.*, 77 (1996) 3865.

[5] F.A.A.I.L. V. Anisimov, First-principles calculations of the electronic structure and spectra of strongly correlated systems the LDA+ U method, *J. Phys-Condens. Mat.*, 9 (1997) 767.

[6] V.V. Anisimov, J. Zaanen, O.K. Andersen, Band theory and Mott insulators: Hubbard U instead of Stoner I, *Physical review. B, Condensed matter,* 44 (1991) 943-954.

[7] Y. Liu, Y. Zhao, Y. Sun, J. Cao, H. Wang, X. Wang, H. Huang, M. Shao, Y. Liu, Z. Kang, A 4e−−2e- cascaded pathway for highly efficient production of H_2 and H_2O_2 from water photo-splitting at normal pressure, *Appl. Catal. B-Environ.*, 270 (2020) 118875.

[8] C. Liu, Y. Fu, Y. Xia, C. Zhu, L. Hu, K. Zhang, H. Wu, H. Huang, Y. Liu, T. Xie, J. Zhong, Z. Kang, Cascaded photo-potential in a carbon dot-hematite system driving overall water splitting under visible light, *Nanoscale*, 10 (2018) 2454-2460.

[9] H.V. Jörn Pommerehne, Werner Guss, Rainer F. Mahrt, Heinz Bässler, Michael Porsch, Jörg Daub, Efficient two layer leds on a polymer blend basis, *Adv. Mater.*, 7 (1995) 551-554.

[10] Q. Wang, M. Nakabayashi, T. Hisatomi, S. Sun, S. Akiyama, Z. Wang, Z. Pan, X. Xiao, T. Watanabe, T. Yamada, N. Shibata, T. Takata, K. Domen, Oxysulfide photocatalyst for visible-light-driven overall water splitting, *Nat. Mater.*, 18 (2019) 827-832.

[11] O. Kiyonori, I. Akio, T. Kentaro, T. Kenji, H. Michikazu, D. Kazunari, Lanthanum–Indium oxysulfide as a visible light driven photocatalyst for water splitting, *Chem. Lett.*, 36 (2007) 854-855.

[12] Y. Li, G. Ma, S. Peng, G. Lu, S. Li, Photocatalytic H_2 evolution over basic zincoxysulfide ($ZnS_{1-x-0.5y}O_x(OH)_y$) under visible light irradiation, *Appl. Catal. A-Gen.*, 363 (2009) 180-187.

[13] H. Abdullah, N.S. Gultom, D.-H. Kuo, Indium oxysulfide nanosheet photocatalyst for the hexavalent chromium detoxification and hydrogen evolution reaction, *J. Mater. Sci.*, 52 (2017) 6249-6264.

[14] X. Chen, H. Sun, D.-H. Kuo, A.B. Abdeta, O.A. Zelekew, Y. Guo, J. Zhang, Z. Yuan, J. Lin, Spherical nanoflower-like bimetallic $(Mo,Ni)(S,O)_{3-x}$ sulfo-oxide catalysts for efficient hydrogen evolution under visible light, *Appl. Catal. B-Environ.*, 287 (2021) 119992.

[15] X. Chen, T. Huang, D.-H. Kuo, H. Sun, P. Li, O.A. Zelekew, A.B. Abdeta, Q. Wu, J. Zhang, Z. Yuan, J. Lin, Material design with the concept of solid solution-type defect engineering in realizing the conversion of an electrocatalyst of NiS_2 into a photocatalyst for hydrogen evolution, *Appl. Catal. B-Environ.*, 298 (2021) 120542.

[16] Z. Gu, J. Qian, R. Wang, M. Lv, X. Xu, Ch. Luo, Aurivillius compound $Bi_5Ti_3CrO_{15}$ as a visible-light-active photocatalyst for hydrogen production from water, *J. Energy Chem.*, 62 (2021) 572-580.

[17] M. Li, J. Sun, G. Chen, S. Yao, B. Cong, P. Liu, Construction photothermal/pyroelectric property of hollow FeS_2/Bi_2S_3 nanostructure with enhanced full spectrum photocatalytic activity, *Appl. Catal. B-Environ.*, 298 (2021) 120573.

[18] M. Li, J. Sun, B. Cong, S. Yao, G. Chen, Sulphur vacancies modified $Cd_{0.5}Zn_{0.5}S/Bi_2S_3$: Engineering localized surface plasma resonance enhanced visible-light-driven hydrogen evolution, *Chem. Eng. J.*, 415 (2021) 128868.

[19] Q. Zhang, Y. Li, H. Ren, Q. Zhai, C. Zhang, L. Cheng, Engineering full hollow and yolk-shell structures of Z-scheme photocatalysts for advanced hydrogen production, *Chem. Eng. J.*, 408 (2021) 127267.

[20] A. Iwase, Y.H. Ng, Y. Ishiguro, A. Kudo, R. Amal, Reduced graphene oxide as a solid-state electron mediator in Z-Scheme photocatalytic water splitting under visible light, *J. Am. Chem. Soc.*, 133 (2011) 11054-11057.

[21] S. Mandal, R. Ananthakrishnan, Double effects of interfacial Ag nanoparticles in a ZnO multipod@Ag@Bi_2S_3 Z-Scheme photocatalytic redox system: Concurrent tuning and improving charge-transfer efficiency, *Inorg. Chem.*, 59 (2020) 7681-7699.

[22] Q.A. Drmosh, A. Hezam, A.H.Y. Hendi, M. Qamar, Z.H. Yamani, K. Byrappa, Ternary $Bi_2S_3/MoS_2/TiO_2$ with double Z-scheme configuration as high performance photocatalyst, *Appl. Surf. Sci.*, 499 (2020) 143938.

[23] H. Lin, K. Zhang, G. Yang, Y. Li, X. Liu, K. Chang, Y. Xuan, J. Ye, Ultrafine nano 1T-MoS_2 monolayers with NiO_x as dual co-catalysts over TiO_2 photoharvester for efficient photocatalytic hydrogen evolution, *Appl. Catal. B-Environ.*, 279 (2020) 119387.

[24] Y. Xu, J. Xu, W. Yan, H. Tang, G. Tang, Synergistic effect of a noble metal free MoS_2 co-catalyst and a ternary Bi_2S_3/MoS_2/P25 heterojunction for enhanced photocatalytic H_2 production, *Ceram. Int.*, 47 (2021) 8895-8903.

[25] C. Chang, C. Huang, Y. Yu, M. Teng, C. Chiang, Y. Lin, Electron transfer dynamics and enhanced H_2 production activity of hydrangea-like $BiOBr/Bi_2S_3$-based photocatalysts with Cu-complex as a redox mediator, *Appl. Surf. Sci.*, 576 (2022) 151870.